LAWRENCE
LIVERMORE
NATIONAL
LABORATORY

UCRL-JRNL-208003

Implosion Hydrodynamics of Fast Ignition Targets

R. B. Stephens, S. P. Hatchett, M. Tabak, C. Stoeckl, T. C. Sangster, R. Petrasso, H. Shiraga, S. Fujioka, K. A. Tanaka

November 15, 2004

Physics of Plasmas

Implosion Hydrodynamics of Fast Ignition Targets

R.B. Stephens[1], S.P. Hatchett[2], M. Tabak[2], C. Stoeckl[3], T.C. Sangster[3], R. Petrasso[4], H. Shiraga[5], S. Fujioka[5], and K.A. Tanaka[5]

[1]General Atomics, San Diego CA 92121
[2]Lawrence Livermore National Laboratory, Livermore CA
[3]Laboratory for Laser Energetics, University of Rochester, Rochester NY
[4]Massachussetts Institute of Technology, Cambridge MA
[5]Institute for Laser Engineering, Osaka University, Osaka, JAPAN

Abstract

The fast ignition (FI) concept requires the generation of a compact, dense, pure fuel mass accessible to an external ignition source. The current baseline FI target is a shell fitted with a reëntrant cone extending to near its center. Conventional direct or indirect drive collapses the shell near the tip of the cone and then an ultra-intense laser pulse focused to the inside cone tip generates high-energy electrons to ignite the dense fuel. We have theoretically and experimentally investigated the collapse of such targets, validating modeling and exploring the tradeoffs available, in such an asymmetric geometry, to optimize compaction of the fuel and maintain the integrity of the cone. The collapse is complex. Away from the cone, the shell collapses much as does a conventional implosion, generating a hot, low-density inner core. But because of the open side hot plasma exhausts out toward the tip of the cone. This hot plasma is advantageous for implosion diagnostics; it can provide protons for angular dependent measurements of the shell wall, neutrons for temperature measurements, and self-emission for contamination measurements. But for FI it is a liability; the hot, low-density inner core impedes the compaction of the cold fuel, lowering the implosion/burn efficiency and the gain. We discuss approaches to optimizing this shell design.

1. Background

The physical outlines of Fast Ignition Fusion (FI) have been known for at least 10 years. [Bas92, Tab94], and the basic requirements are well known [Atz99, Ros99]. It differs from the conventional central-hot-spot (CHS) approach in using separate drivers for the compression and ignition steps. This eliminates the need for a shock-heated low-density ignition spot surrounded by a high-density core and allows compression of the target to a uniform density ~ 1/3 and an ignition mass ~ 1/10 that required by the CHS approach; the consequent reduced energy input results in a very attractive improvement in target gain.

In the initial concept [Tab94] the ignition pulse is provided by an ultra-high-intensity laser that bores into the lower density plasma surrounding the assembled target as far as the relativistic critical density surface. There its energy is converted into electrons that travel the rest of the distance to the dense (~300 g cm^{-3}) core of the target. Since the critical surface, from which these electrons would be launched, is located many hundreds of microns from the core, a variant target design containing a reëntrant cone was introduced to allow electron generation closer to the core [Tab97, Kod01]. Small-scale integrated experiments have shown short-pulse laser heating efficiency of ~25% [Kod02]. But the details of the collapse, particularly modifications caused by possible interactions between cone and shell, were unknown.

We have carried out a series of combined experiments and simulations designed to establish a detailed understanding of the compression of a reëntrant cone fast ignition target. There were three major questions to address: 1) do the hydrodynamics codes, which have been exhaustively tested on spherically symmetric targets, properly capture all of the physics in these extremely asymmetric cases, 2) do shell-cone interactions interfere with efficient assembly of a dense core, and 3) does the design space allow simultaneous core assembly and ignition access.

Initial modeling (§2) showed that the generation of the desired uniformly dense blob of fuel was difficult; the hot central core is a robust feature. Then several combined experimental/modeling campaigns (§3) showed reasonable efficiency in assembling a core but also a number of shell-cone interactions that must be accounted for during optimization. We discuss the various interactions in §4. Using this information, we then describe requirements regarding FI target optimization (§5). We conclude (§6) that though the simulations are qualitatively accurate, mixing—which is omitted—is an important process shaping the collapse properties, and that there are substantial cone-shell interactions that considerably

complicate the problem of developing an optimized target. Our modeling has, however, established promising directions as the foundation of a concerted design effort.

2. Initial Modeling

The first simulation (Fig. 1), used a typical CHS shell and drive with a cone added (the hyperboloidal tip offset from the shell center by ~40 μm) and with minimal central gas (ρ_{gas} =5×10^{-5} g cm^{-3}). This target collapses to a hollow shell around a low-density core. The gas is generated by the shock from the laser drive and then, because the shell collapses faster than it can escape, is heated to ~400 eV by compression. Although the maximum areal density of this target (ρR~2.2 g cm^{-2}) is satisfactory, the extended form this target takes at stagnation is undesirable. Unlike a CHS target, a FI target does not burn from the center out starting at the low-density core. Rather ignition occurs in the dense shell, and the resulting nuclear burn, limited to dense fuel, must travel along the thin shell. Improved collapses can be formed by generating a larger collapse velocity from the side away from the cone than at the sides, using either an ablator, fuel, or drive asymmetry (Fig. 2). A symmetric target (as in Fig 1) with a 10% drive asymmetry produces a much more satisfactory shape with the same ρR (Fig. 2c). Injection of ad hoc electron beams suggest this mass has a reasonable chance of being ignited, yielding >20 MJ after ignition with between 30 and 150 kJ of 1 MeV electrons, for electron beam divergence of 0° and 50° respectively [Steve - add ignition figure? – see optional Fig. 2.5 in ppt]. Capsules tuned for lower drive temperature or energy produced ρRs less than 2 g cm^{-2}, and proved much harder to ignite. The collapse geometry changes rather strongly with scale size (Fig. 3); considerable work will be required to optimize this type of target.

3. Experimental tests

The cryo-ignition target in Fig. 1 was then re-sized to Omega scale, first for x-ray drive [Ste03] and then for direct laser drive [Sto04], to test the model predictions. X-ray drive targets (Fig. 4a) were driven exactly as a 1/2 mm dia CHS shell in a scale 1 hohlraum using 14 kJ of drive power. The reëntrant cone was notched outside the shell to prevent an excessive x-ray flux on the cone near the shell. The direct drive targets had a ~ 1 mm diameter shell (Fig. 4b). The cone base blocked one set of beams entirely. The shell was driven with 11 kJ from 15 half power and 20 full power beams. In the cases illustrated here the targets were backlit with He-like Fe-K_α radiation (6.7 keV) from a film hit with delayed beams (8 beams delayed 1.4 ns on the outside of a 7 μm foil for x-ray drive and 15 beams, delayed 1.8 ns on both sides of a 25 μm foil for direct). The sensitivity of the framing camera was determined by reference to a calibrated time integrating x-ray spectrometer [Bur83]. The emitted spectrum, convoluted with the camera filter transmission and the spectral sensitivity of the camera [Bur92], was compared to the backlighter intensity integrated over backlighter area (a vertical and horizontal super-Gaussian fit was used to account for the part of the backlighter hidden behind the target) and summed over the camera frames.

The tests were made with nominally symmetric targets and symmetric drives, so we expected a collapsed geometry as in Fig. 1. A collapsed x-ray drive target is shown in Fig. 5 and direct drive targets in Fig. 6. Targets were either empty or filled with 5-10 atm D_2. In all cases the cone (with an initially sharp, hyperboloidal tip Fig. 5b) appears distorted. For the x-ray drive case (Fig. 5) there appears to be no separation between the shell and the cone. For direct drive (Fig. 6) the separation is too bright to be completely real. Gas-filled targets showed obvious self-emission near stagnation. Detailed investigation of these images revealed a number of shell-cone interactions occurring in fast ignition targets that must be taken into account in their design.

4. Cone-shell interactions

4.1 Cone heating/Au contamination

The fuzziness of the cone outlines in the back-lit images (especially in x-ray drive, Fig. 5) is caused by a surrounding cloud of Au vapor. An unintentional high-photon-energy component of the drive spectrum is boiling away the Au surface. The origin of the x-rays, in the x-ray drive case, comes from the non-thermal Au-M lines in the emission from the Au hohlraum (~6% of the total incident energy for our targets [Ame03]), and from hot-electron-created bremstrahlung in the direct drive case. In a CHS target these weakly absorbed spectral components cause a mild preheating of the imploding shell. In a reëntrant cone FI target, such penetrating radiation (~1.5-4.5 keV with peak at 2-2.5 keV) is absorbed by the surface of the

cone. LASNEX calculations suggest that the energy incident on the cone is ~40 kJ cm^{-2} in the x-ray drive case and ~ 9 kJ cm^{-2} for direct drive. In neither case is that flux easily eliminated. For x-ray drive, all of the possible hohlraum materials used for hohlraum materials emit non-thermal lines in the same energy band. For direct drive the bremstrahlung induced by the laser-generated-hot-electrons scales with Z^2 of the shell material; it would be reduced somewhat with a Be:Cu_x shell and considerably more using a cryo-foam target (that reduces the C density by nearly an order of magnitude).

This incident energy, absorbed in <1 μm of the Au, generates a dense vapor layer (~0.5 g cm^{-3} – clearly seen in the first images of Fig. 7) that is Rayleigh-Taylor (R-T) unstable against the pressures exerted by the lower density gas escaping the collapsing shell, so mixes with it. In the x-ray drive case a filament of Au vapor can be seen to escape into the low density core (Fig. 5b). The apparent contamination is much more limited in our direct-drive experiments. The extent of that contamination cannot be measured with opacity, as in indirect drive, because of self-emission (s-e) from the hot core. This s-e is as bright as the backlighter in some cases and gives the illusion of a complete separation between cone and collapsed shell (as in Fig. 6a) unless a whole sequence is examined (Fig. 7).

Within the collapsing shell, LASNEX simulations qualitatively replicate the time evolution and shape of the s-e as well as the evolving shape of the target, but overestimate the absolute value of both s-e and opacity. The maximum s-e intensity varies at least a factor of 2 from shot to shot. Since the framing camera only detects hν >2 keV >> kT, the measured intensity is extremely sensitive to the gas temperature; a reasonable assumption is that mixing, varying with laser drive, target surface and axial symmetry deviations, is the cause of both the low s-e intensity and the variability (Fig. 6b,c).

Near the cone, the simulations are not so accurate. They predict a sharply defined Au vapor layer that is not pushed back until near the stagnation time, and no s-e; we observe no boundary and rather bright s-e (Fig. 7). As noted above, the Au vapor boundary is R-T against the CH gas stream, so would be expected to mix. Any Au contamination increases the opacity of the gas in that vicinity (H is invisible and the C is ionized enough to lower its normal absorption by orders of magnitude in the low density exhaust gas), and thus the s-e brightness. A comparison of simulated and observed s-e plotted along the cone axis (Fig. 8) indicates the mixing length of the Au vapor. By this measure, the Au is detectable about halfway from the tip of the cone toward the core of the shell.

4.2 Shell-cone asymmetry

The addition of a reëntrant cone put a new requirement that the shell collapse to a pre-determined point in front of the cone tip. A cone offset more than ±10 μm causes turbulent mixing of the core with the wall and prevents an optimum collapse (Fig. 6c,d). Such an offset can be caused by asymmetric drive, or shell, mis-placement or -orientation in the target chamber. It appears, in this case, that the cone axis was tilted ~ 5° from nominal. Since the beams under the cone are not used, this turned part of the shell toward lower intensity drive and shifted the center of collapse.

4.3 Cone collapse

The cone seen in indirect drive experiments (the opaque region in Fig. 5) appears considerably blunted compared to its original shape. That is to be expected; the central gas (according to simulation a density of ~xx g cm^{-3}, heated to ~400 eV, and moving at ~ 10^5 cm sec^{-1}) [Steve – are these numbers correct?], is flowing directly toward the tip, eventually punching it in, as seen in Fig. 2. Since it is through that tip that the ignition energy is transmitted, the timing of that collapse is of some interest. The simulated backlit images show that qualitatively through the position of the Au vapor; the boundary is not pushed down against the tip until just before stagnation. Experimentally, that layer vanishes somewhat earlier (Fig. 7 simulation image 3 and experimental image 1, respectively). This was investigated quantitatively using the shadow of a ledge partway down the cone as a stable reference point (Fig. 9a). Fitting all the images in each shot to a 3-D model allowed determination of the fixed parameters in a sequence, and the height of each cone tip above its ledge as a function of time (Fig. 9b). The measured collapse rate agrees quite well with that predicted by simulation. Both indicate that the tip collapses by 20-30 μm before stagnation—more than the expected cone tip thickness—so the tip would be destroyed by the time of the ignition pulse.

5. Fast ignition target optimization

5.1 High-Z doping of core gas

High-Z doping of the core gas might do no harm, since the low-density fuel is not burned in a FI target, and might actually do some good, by allowing the core to radiatively cool, lowering its pressure and allowing the surrounding shell to collapse to a smaller, more compact core. Allowing such doping puts a premium on minimizing the mixing between the hot core and collapsing shell, so the specifications on the drive and shell for an FI target could be nearly as rigorous as those for a CHS target. If necessary, such doping could be suppressed by tamping the high-Z cone surface with a thin plastic or low-Z metal covering.

5.2 Shell-cone asymmetry

Simulations suggested that offsets $<\pm 10$ μm were acceptable. All targets were built to that specification, and most collapsed cores were satisfactorily aligned to their cone. Most potential sources of offset (drive imbalance and target placement) are also potential problems in standard CHS shells and well enough controlled that they are not a problem [private commun. D.D. Meyerhofer]. There is a new requirement for FI targets; apparently the cone axis alignment must be controlled to $\sim\pm 1°$; that is not difficult to achieve. However building the target with sufficient accuracy is, and will remain a challenge.

5.3 Cone collapse

The observed cone collapse ≥ 30 μm before stagnation is a serious problem as it is large enough to destroy the tip before the ignition pulse arrives, strongly affecting the conditions in with the electron or proton beam is produced. It is a direct consequence of the formation of a hot, (relatively) low-density core in the collapsing target (even in an initially empty shell). Using an asymmetric drive to compress it away from the cone stretches the dense shell into an extended shape that is not conducive to an efficient burn; compressing it toward the cone makes a more compact fuel core, but impacts the cone even more strongly (Fig. 3b). A study of the cone collapse as a function of drive symmetry is necessary to establish the optimum configuration.

6. Conclusions

A reëntrant cone FI target can be collapsed with around half the efficiency of a reentrant cone target simulation, depending on the parameter of interest (Table 1). The disparity is presumably the result of mix—an important process in cone-targets—not included in the simulation. Although these parameters are calculated from locations away from the cone, they cannot be easily compared to a 1-D CHS implosion; the gas escape in allowed by the presence of the cone, and only modeled by a 2-D calculation, allows these targets to collapse to a more compact kernel than otherwise (Table 1).

The requirements for optimizing such a target are rather different and perhaps not much less stringent than for CHS. Targets must be assembled with high precision. High mode asymmetries must be controlled to limit mixing of contaminated core gas with the dense fuel to be burned. Low mode asymmetries must be controlled to place the compressed fuel at the correct place ± 10 μm and to control the strength of gas flows impacting the cone tip. Withal, the design space available to FI target design is huge, and we have just begun to explore the possibilities.

Acknowledgments

The authors are indebted to the target fabrication group at GA and the OMEGA staff at LLE for making these experiments possible. We are grateful to Dr. S.G. Glendinning (LLNL) for evaluating the drive beam imbalance in our experiments (there wasn't any) and to B. Yaakobi (LLE) for calibrated spectrometer measurements. This work was supported by the U.S. Department of Energy Office of Inertial Confinement Fusion under Cooperative Agreement No. DE-FC03-92SD19460, the University of Rochester and the New York State Energy Research aned Development Authority and with the corporate support of General Atomics. The support of the DOE does not constitute an endorsement of the views expressed in this article.

This work was performed under the auspices of the U.S. Department of Energy by University of California, Lawrence Livermore National Laboratory under Contract W-7405-Eng-48.

References

Ame03 – P. Amendt and R. Turner, unpublished.
Atz99 – S. Atzeni, *Phys. Plasmas* **6**, 3316 (1999).
Bas92 – N.G. Basov, S.Y. Guskov and L.P. Feokistov, *J. Sov. Laser Res.* **13**, 396 (1992).
Bur83–A. J. Burek and B. Yaakobi, NTIS # DE83015439 9A (1983).
Bur92 – G.A. Burginyon et al., *SPIE* **1736**, 36 (1992).
Kod01 – R. Kodama et al., *Nature* **412**, 798 (2001).
Ros99 – M. Rosen, *Phys. Plasmas* **6**, 1690 (1999).
Ste03 – R.B. Stephens et al., *Phys. Rev. Lett.* **91**, 185001 (2003).
Sto04 – C. Stoeckl et al., submitted to *Phys. Rev. Lett.* in 2004.
Tab94 – M. Tabak et al., *Phys. Plasmas* **1**, 1626 (1994).
Tab97 – M. Tabak et al., U.S. Patent #xxxxxxx (1997).

Figures for Implosion Hydrodynamics mss

Rev 3 - 11 Nov

Figure 1: NIF scale reëntrant cone fast ignition target designed to absorb ~ 180 kJ of $T_{rad,max}$=250 eV radiation and be imploded to <rR>DT~2.2 g cm^{-2}. The initial central gas density is $3 \cdot 10^{-5}$ g cm^{-3}, and the cone tip is offset from the shell center by ~40 μm.

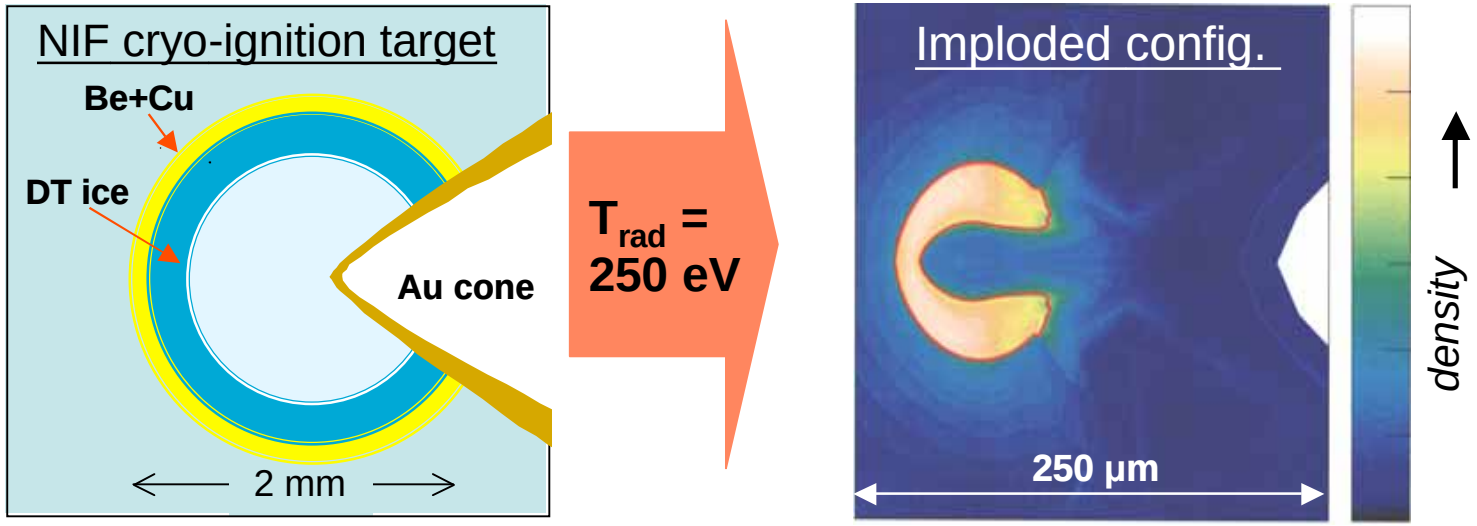

Figure 2: Cross-section of imploded capsule density from target as in Fig. 1 but with a polar asymmetry in the collapse: a) the ablator was 10% thinner on the side away from the cone, b) the fuel was 10% thinner on the far side, and c) the target was uniform but the intensity was ~10% higher on the far side. The stagnated targets have ρR~1.8, 2.2, and 2.2 g cm^{-2}, respectively.

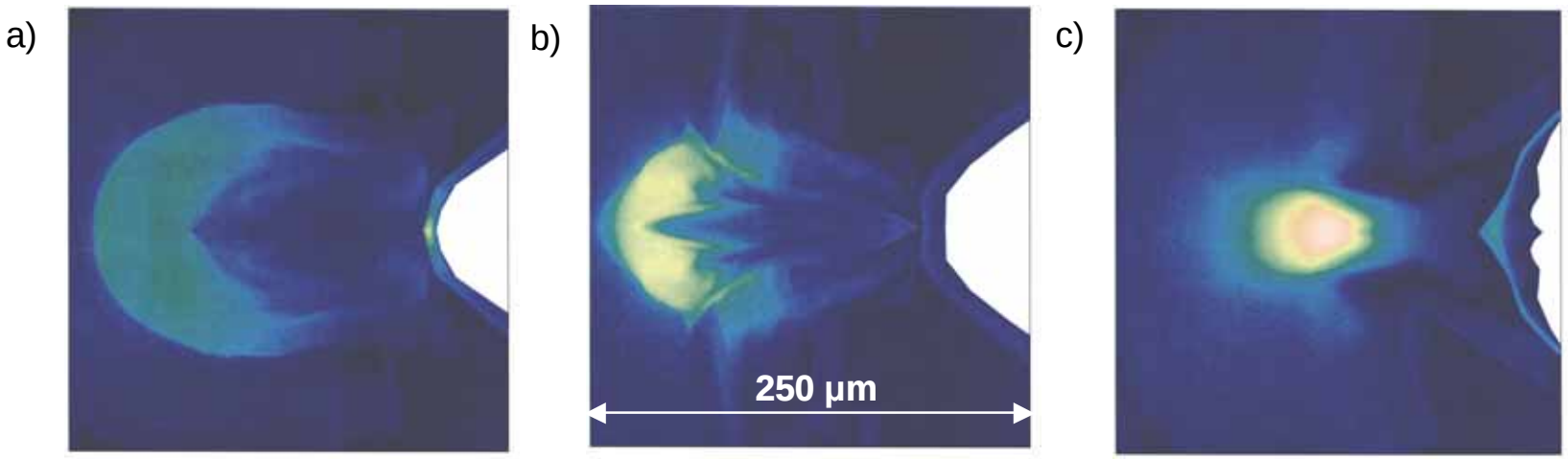

Figure 2.5: Electron beam ignition of the compressed fuel in Fig. 2c. The beam was given a spread of 50° fwhm in a) and c), and 0° radius 20 μm in b) and d). A) and b) show energy deposition per mass, c) and d) show neutron yield at the end of energy deposition. The 50° (0°) fwhm beam required E_{beam} ~ 150 kJ (30 kJ) for ignition and yielded 24 MJ (27 MJ).

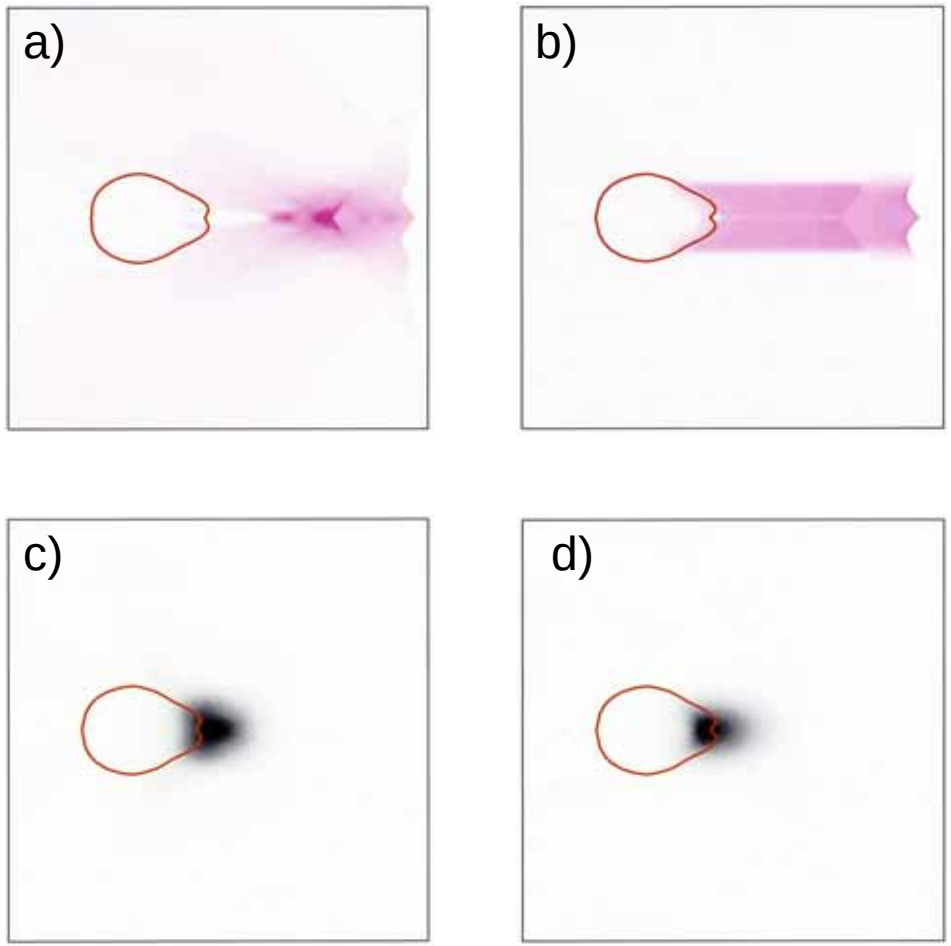

Figure 3: Target from Fig. 1 scaled up 1.6X and driven at $T_{R,\,max}$=190 eV, absorbing 380 kJ in 42 ns a) symmetrically and b) with 10% polar asymmetry.

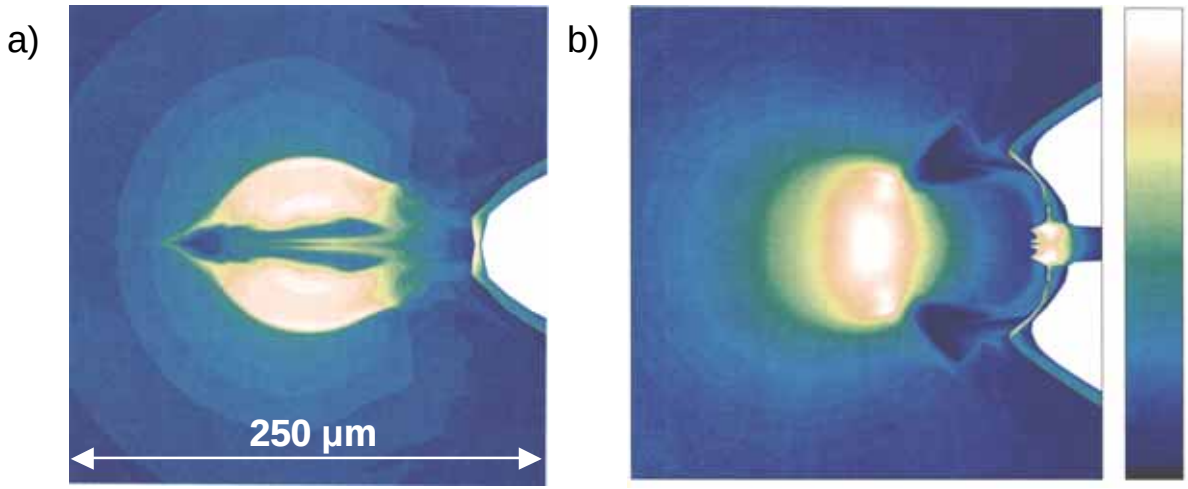

Figure 4: Realizations of reëentrant cone fast ignition targets for a)x-ray drive and b) direct laser drive on Omega.

a)

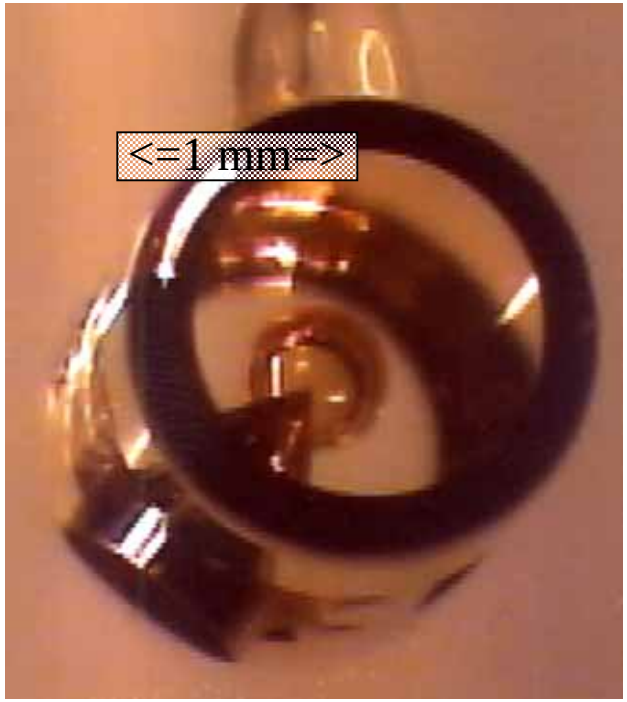

b)

Figure 5: Back-lit x-radiograph images of x-ray drive targets at stagnation with a) linear and b) log grey scale, and c) simulation using linear grey scale. The experiment, unlike the simulation, shows a thread of opaque material leaking from the cone into a dense shell center. In b) the thin colored line shows the original shape of the cone, the thick white line shows the border of the completely opaque region. All the images are to the same scale.

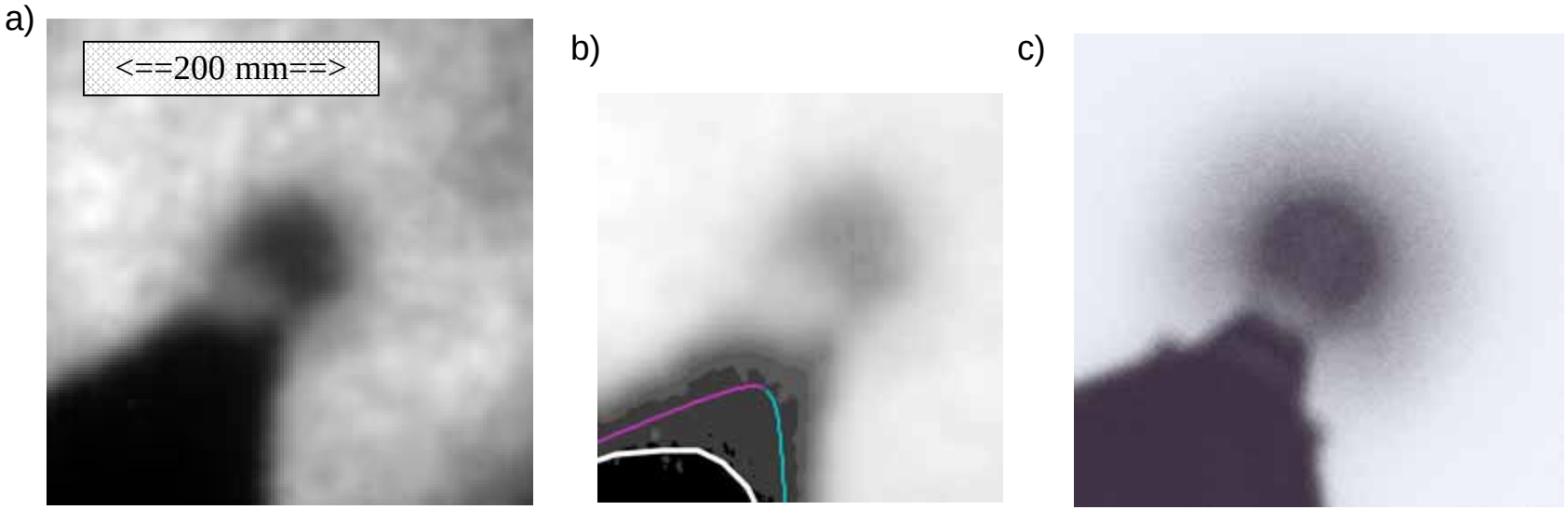

Figure 6: Back-lit x-radiograph images of direct drive targets at stagnation a) with only V filter to show self-emission, b) with Fe filter to (largely) eliminate self-emission, c) with same filter and off-center collapse. Each contained ~ 5 atm D_2. Cone and core centerlines are drawn in b) and c) as guides to show the ~25 μm offset in c). d) Lineouts across the images in b) and c) showing that the offset limited the compression (FWHM increased from 80 to 120 μm), and reduced core gas self-emission (the apparent absorbed fraction increased from 0.65 to 0.75).

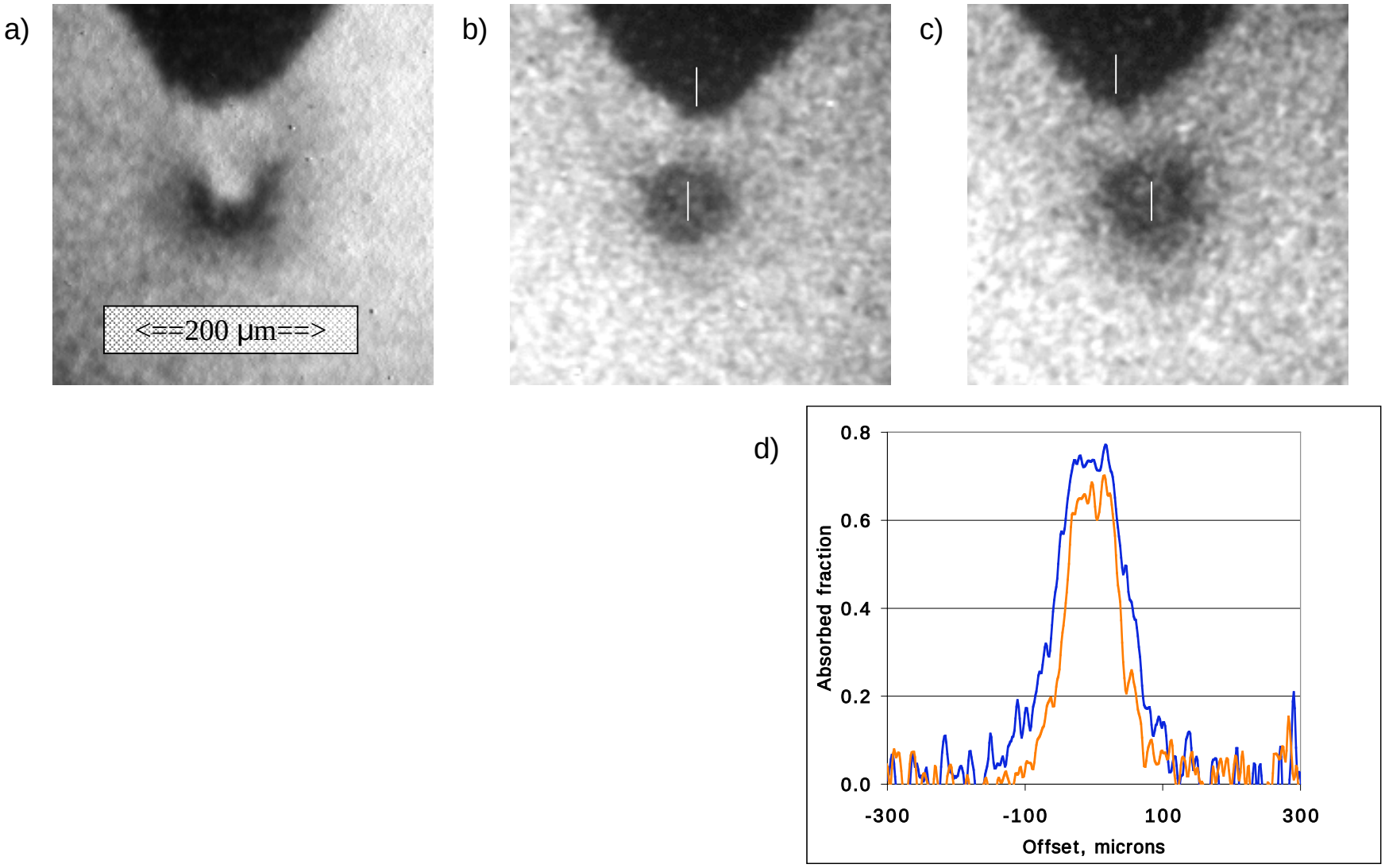

Figure 7: Sequence of direct drive collapse images from a) experimental shot #32387 and b) simulated in LASNEX. The simulated images assumed a backlighter brightness ~ 2.5×10^9 photons/sr/cm^2/ns.

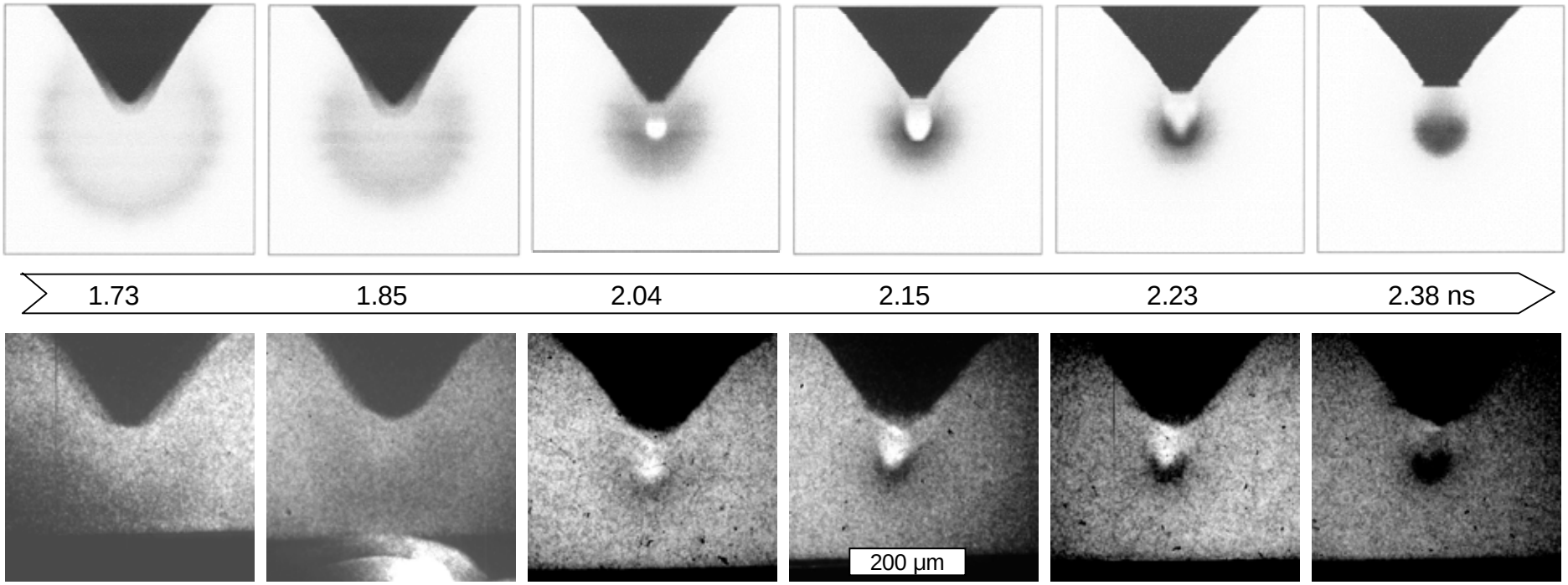

Figure 8: x-ray Images of a shell near the s-e maximum at a) 2.3 and b) 2.35 ns (stagnation was ~2.4 ns) from images viewed through a V filter (detecting ~ 5 keV) and backlit with Fe (6.7 keV) (shot #35693). The dim backlight shows the cone position (the bases indicated by solid lines) but does not interfere with s-e. b), c) Lineouts along the cone axis from images shown in a), b) vertically averaged within the pairs of dotted lines. The tip of the cone is on the LHS of each graph. Lineouts derived from LASNEX simulations are dashed; their intensities scaled to match the experimental value near the center of the target. Excess emissions between the cone and s-e maximum are attributed to the presence of Au vapor.

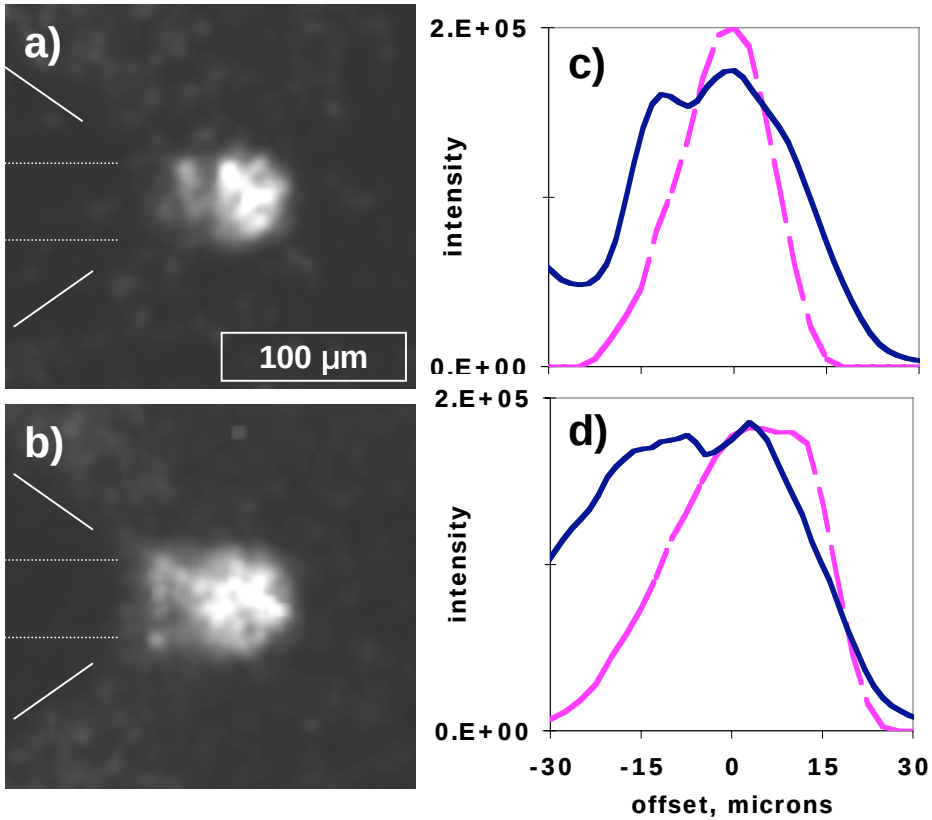

Figure 9: a) The actual tip height was calculated by fitting the shadow of the ledge to an ellipse whose orientation and size was held fixed for all images in a sequence and assumed to be centered under the tip. b) Calculated tip height vs time for filled(triangles) and capsules (squares and Xs), and from LASNEX simulation of a gas filled capsule (smooth line).

a)

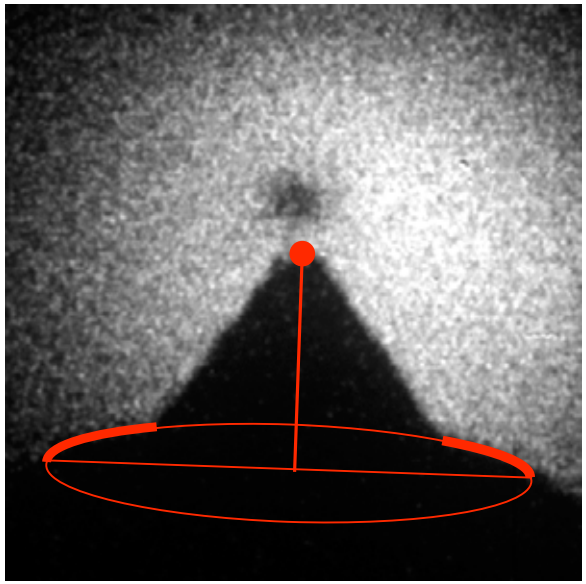

b)

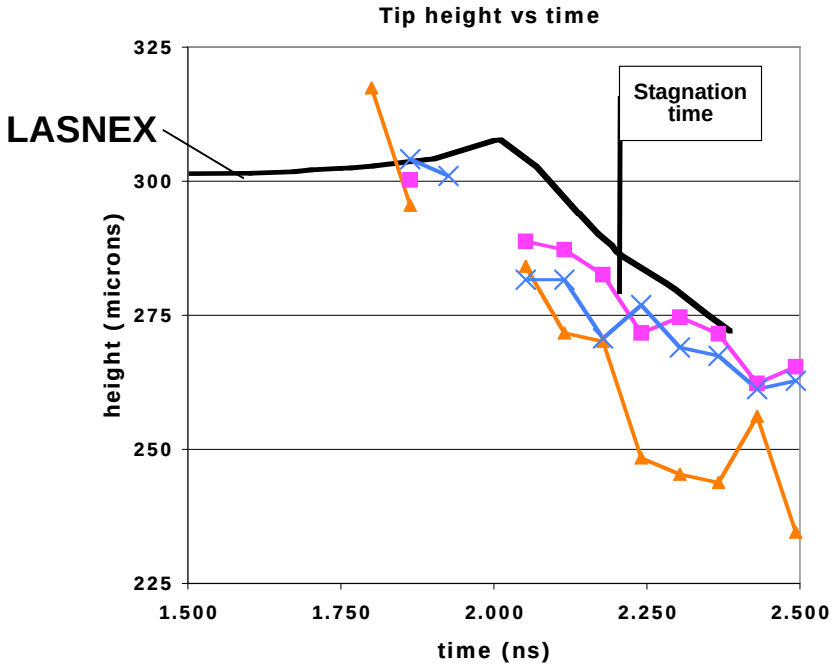

Table 1: Collapse metrics as measured experimentally for direct and indirect drive, and as predicted by LASNEX simulations for a reëntrant cone shell. According to the simulation, it fares better than a CHS shell collapsed under the same conditions; perhaps because the core can leak out, allowing collapse to a smaller size.

	Experiment	**Simulation**	
	Cone-Shell		Sphere
ρ_{max} (gm/cc):	20/15-20	68-100/60	40/46
ρR (mg/cm^2):	70/70-100	200/130	150/130
m/m_o:	0.3/0.1-0.2	0.42-0.43/0.32	0.47/0.33

(x-ray/laser drive)